Eur. Phys. J. B **60**, 161–169 (2007)
DOI: 10.1140/epjb/e2007-00339-4

THE EUROPEAN PHYSICAL JOURNAL B

Magneto-electronic properties of the AA- and ABC-stacked graphites

C.L. Lu[1,a], C.P. Chang[2,3,b], and M.F. Lin[1,3,c]

[1] Department of Physics, National Cheng Kong University, 701 Tainan, Taiwan
[2] Center of General Education, Tainan University of Technology, 710 Tainan, Taiwan
[3] National Center for Theoretical Sciences, 701 Tainan, Taiwan

Received 10 August 2007 / Received in final form 17 October 2007
Published online 8 December 2007 –

Abstract. In this study, we apply the tight-binding method to magneto-electronic properties of the AA- and ABC-stacked graphites, which are strongly dependent on the interlayer interactions, the magnetic field, and the stacking sequences. First of all, the interlayer interactions induce the significant changes in the energy dispersions, the band symmetry about the Fermi level, the overlap between valence and conduction bands, the band width, and the band-edge states or the symmetry points. Then, the magnetic field induces the Peierls phase in the Bloch functions and thus strongly affects the energy dispersions of the Landau Levels, the subband spacings, the energy width, and the special structures in density of states (DOS). Finally, the stacking sequences dominates over the low-energy band overlap and the anisotropy of energy bands. The effects mentioned above are exactly reflected in the density of state. Here, DOS exhibits the 3D, 2D, and 1D characteristics.

PACS. 71.10.-w Theories and models of many-electron systems – 71.20.-b Electron density of states and band structure of crystalline solids – 71.70.Di Landau levels

1 Introduction

Graphite, which is one of the most important layered systems, has attracted a lot of theoretical [1–12] and experimental [13,14] studies. There are four kinds of the layered graphites, the simple hexagonal graphite (the AA-stacked graphite) [6], the Bernal graphite (the AB-stacked graphite) [7,8], the rhombohedral graphite (the ABC-stacked graphite) [9–11], and the turbostratic graphite (without the periodical stacking sequence) [9]. The AB-stacked system is the common structure of the layered graphite. The natural and synthesized graphites are found to contain varying amounts of the ABC-stacked graphite. For example, the magnetic properties of mixed graphite sample containing increasing volume-fractions, up to ≈40%, of the rhombohedral phase are investigated [15]. The graphite intercalation compounds, e.g., the Li intercalated graphite, might exhibit the AA stacking sequence. The turbostratic graphite might exist in bad experimental samples. Recently, the appearance of the AA- and ABC-stacked structures on the graphite surface, where the graphite superlattices form, has been reported [16]. And, the monolayer, bilayer, and trilayer graphites have been produced due to the progress of the fabrication [17–21]. Such pure 2D systems are identified to display very interesting physical properties, e.g., the novel quantum Hall effect [20–22]. Electronic states and Landau levels in graphene stacks, including the AB and ABC stackings, are theoretically studied [23]. The above-mentioned studies show that the stacking effect influences the physical properties of these allotropic materials. In this work, we mainly focus on the magneto-electronic properties of the AA- and ABC-stacked graphites.

A monolayer graphite has the hexagonal symmetry; therefore, the low-energy π-electronic structure, due to the $2p_z$ orbitals, exhibits the special zero-gap characteristic [1]. The linear conduction and valence bands just intersect at the Fermi level, so that the density of states is vanishing at $E_F = 0$. The free carriers are absent in a monolayer graphite. There exist the van der Waals interactions between the graphitic layers in the layered systems. The interlayer atom-atom interactions (the interlayer atomic hopping integrals) would play an important role in the π-electronic properties, e.g., energy dispersions, free carriers, and band width. They are different in the AA- and ABC-stacked graphites, and so are the π-electronic properties.

Some studies on magneto-electronic properties of a monolayer graphite [24–26] and the AB-stacked

[a] e-mail: lu.chilang@gmail.com
[b] e-mail: t00252@mail.tut.edu.tw
[c] e-mail: mflin@mail.ncku.edu.tw

graphite [27] are reported. When the graphitic systems are present in a uniform magnetic field along the z-axis, the magnetic flux would induce a Peierls phase in the Hamiltonian. This phase could significantly modify the π-electronic structures. The previous studies [26] predict that there are oscillating Landau levels, and complete flat or partial flat Landau levels. Such Landau levels are further reflected in optical properties, e.g., a lot of prominent absorption peaks with the special divergent structures [26]. The comparison between a monolayer and the AB-stacked graphites shows that the interlayer interactions not only give rise to the anisotropic energy dispersions along the stacking direction but also have a significant effect on the magneto-electronic properties on the graphitic planes, e.g., the change of the feature of Landau levels, the oscillating period of oscillating Landau subbands and the feature of DOS. Therefore, the interlayer interactions are expected to have a strong effect on magneto-electronic properties of the AA- and ABC-stacked graphites.

To evaluate the electronic structures of the AA- and ABC-stacked graphites in the presence of a uniform perpendicular magnetic field, the tight-binding model is used in this work. The wave-vector-dependent energy bands, the butterfly-like energy spectra, and the density of states are calculated. Besides, we have some discussions about electronic properties, energy dispersion, band width, band symmetry about the Fermi level, free carriers, special points in the energy-wave-vector space, Landau levels or oscillating Landau levels, and special structures in DOS systematically. Investigations of the dependence of electronic properties on the interlayer interactions, the magnetic flux, and the stacking sequences are also made in detail. More importantly, we made several comparisons of the electronic structures of the allotropic form of graphite, e.g., the AA-, AB-, and ABC-stacked graphites and a monolayer graphite. This work is organized as follows. In Section 2, energy bands are calculated within the tight-binding model. In Section 3, magneto-electronic properties are discussed. And conclusions are drawn in Section 4. Above all, optical spectroscopy and STM could be used to examine the predicted results.

2 The tight-binding method

A monolayer graphite is composed of the hexagonal carbon rings. The identical graphite layers are arranged periodically along the z-axis to obtain the layered graphites. In this work, we only focus on two kinds of stacking sequences, AA and ABC. The AA-stacked graphite, as shown in Figure 1, has the same (x,y) coordinates for carbon atoms in every layer. The periodical lengths along $\hat{x}$, $\hat{y}$, and $\hat{z}$ are, respectively, $I_x = a = 2.42$ Å, $I_y = 3b/2 = 2.13$ Å, and $I_z = c = 3.35$ Å. A primitive cell contains two carbon atoms (A and B). The first Brillouin zone of the 3D hexagonal structure, as shown in the inset of Figure 3a, possesses high symmetric points $\Gamma(0,0,0)$, $M(\frac{\pi}{a}, \frac{\pi}{3b}, 0)$, $K(\frac{4\pi}{3a}, 0, 0)$, $A(0,0,\frac{\pi}{c})$, $L(\frac{\pi}{a}, \frac{\pi}{3b}, \frac{\pi}{c})$, and $H(\frac{4\pi}{3a}, 0, \frac{\pi}{c})$.

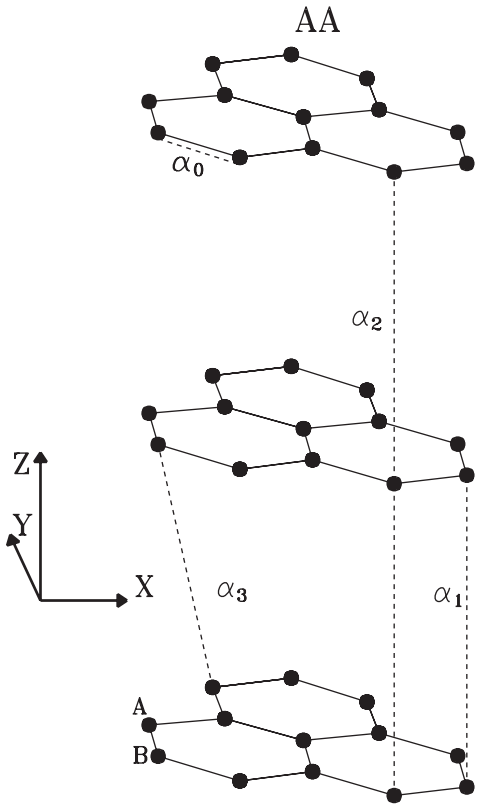

Fig. 1. The geometric structure of the AA-stacked graphite. All the atomic interactions are also shown.

The tight-binding model is used to calculate the π-electronic structure of the AA-stacked graphite. The Bloch function is:

$$\Psi^h_{\mathbf{k}}(\mathbf{r}) = \mathrm{a}\mathbf{\Psi}_{\mathbf{k},A}(\mathbf{r}) + \mathrm{b}\mathbf{\Psi}_{\mathbf{k},B}(\mathbf{r}), \quad (1)$$

in which h represents the subband index. The two tight-binding functions, which are the linear superposition of the periodical $2p_z$ orbits (ψ's) on all layers, are expressed as

$$\Psi_{\mathbf{k},A(B)}(\mathbf{r}) = \sum_{\mathbf{R_j}} \mathrm{a_j}\, e^{i(\mathbf{k}\cdot\mathbf{R_j})} \psi_{A(B)}(\mathbf{R_j} - \mathbf{r} - \tau_{A(B)}). \quad (2)$$

$\mathbf{R_j}$ is the 3D periodical position vector, and τ_A (τ_B) is the position vector in a basis. Two kinds of atom-atom interactions are taken into account. First, the interaction associated with the same atom is the site energy. It is set to zero for the AA-stacked graphite. Second, the interactions between different atoms correspond to the atomic hopping integrals α_i's. $\alpha_1(\alpha_2)$ is the interaction between two A atoms from the two neighboring (next-neighboring) layers. $\alpha_0(\alpha_3)$ represents the hopping integral between A atom and B atom from the same layer (the two neighboring layers). Their values are: $\alpha_0 = 2.569$ eV, $\alpha_1 = 0.361$ eV, $\alpha_2 = 0.013$ eV; $\alpha_3 = -0.032$ eV [8]. The Hamiltonian, which is built in the subspace spanned by the two

tight-binding wave-functions $\Psi_{\mathbf{k},A}$ and $\Psi_{\mathbf{k},B}$, is given by

$$H_{\mathrm{AA}}(\phi=0)= \begin{pmatrix} \alpha_1\beta+\alpha_2(\beta^2+2) & (\alpha_0+\alpha_3\beta)f(k_x,k_y) \\ (\alpha_0+\alpha_3\beta)f^*(k_x,k_y) & \alpha_1\beta+\alpha_2(\beta^2+2) \end{pmatrix}, \quad (3)$$

where ϕ is the magnetic flux. $\beta = 2\cos(k_z c)$ and $f(k_x,k_y)=e^{ik_y b}+2e^{-ik_y b/2}\cos(k_x\sqrt{3}b/2)$. The eigenvalues of equation (3), the energy dispersions, are:

$$E_{\mathrm{AA}}(k_x,k_y,k_z;\phi=0)=\alpha_1\beta+\alpha_2(\beta^2+2)\pm(\alpha_0+\alpha_3\beta) \times\sqrt{1+4\cos(3k_y b/2)\cos(k_x\sqrt{3}b/2)+4\cos^2(k_x\sqrt{3}b/2)} \quad (4)$$

The switching-off of the interlayer interactions (α_1, α_2, and α_3) allows us to obtain the energy dispersions of a monolayer graphite, which are:

$$E(k_x,k_y;\phi=0)= \pm\alpha_0\sqrt{1+4\cos(3k_y b/2)\cos(k_x\sqrt{3}b/2)+4\cos^2(k_x\sqrt{3}b/2)}. \quad (5)$$

The AA-stacked graphite is present in a uniform magnetic field **B** perpendicular to the periodical planes. This field would induce a Peierl's phase in the Bloch function, as expressed by

$$\Psi_{\mathbf{k},A_i}(\mathbf{r})= \sum_j a_j e^{-i[\mathbf{k}\cdot\mathbf{R}+\frac{e}{c\hbar}\int\mathbf{A}(\mathbf{R_j},\mathbf{r})\cdot dr]}\psi_{A_i,j}(\mathbf{R_j}-\mathbf{r}-\tau_A). \quad (6)$$

The vector potential in the Landau gauge is chosen as $\mathbf{A}=(-By,0,0)$. The magnetic flux through a hexagon is assumed to be $\phi=\phi_0/q$, where q is a nonzero integer number and $\phi_0 = hc/e = 7.89\times10^4$ TÅ^2 is the magnetic flux quantum. The magnetic flux causes a new periodicity with period q times that of the tight-binding functions in equation (2). A primitive unit cell, which includes the q zigzag lines along the y-axis in a graphitic plane (Fig. 1), has $2q$ carbon atoms. The first Brillouin zone along the k_x-axis is reduced to $1/q$ of that without ϕ, changing from the hexagonal structure into the orthohomic structure, where the high symmetric points are $\Gamma(0,0,0)$,$X'(\frac{4\pi}{3qa},0,0)$, $M(\frac{4\pi}{3qa},0,\frac{\pi}{c})$, and $Y(0,\frac{\pi}{3b},0)$, respectively (Fig. 4a). Based on the $2q$'s tight-binding functions, the ϕ-dependent Hamiltonian matrix of the AA-stacked graphite is

$$\begin{pmatrix} H_I(1) & H_J & 0 & \cdots & 0 & H_J^* \\ H_J^* & H_I(2) & H_J & 0 & \cdots & 0 \\ 0 & \ddots & \ddots & \ddots & \ddots & \vdots \\ \vdots & \ddots & H_J^* & H_I(m) & H_J & \vdots \\ 0 & \ddots & \ddots & \ddots & \ddots & \ddots \\ H_J & 0 & \cdots & 0 & H_J^* & H_I(q) \end{pmatrix}, \quad (7)$$

in which $H_I(m)$ or H_J is a 2×2 matrix. $m=1,2,3,...q$ denotes the mth zigzag line. The periodical boundary condition $H_J^*(q+1)=H_J(1)$ is included in equation (7). The 2×2 $H_I(m)$, which is spanned by the two Bloch functions associated with A atom and B atom (or two A atoms) from the same or different layers (the different layers) in the mth zigzag line, is given by

$$\begin{cases} H_I(m)_{11}=\alpha_1\beta+\alpha_2(\beta^2+2) \\ H_I(m)_{12}=2(\alpha_0+\alpha_3\beta)e^{-ik_y b/2}\cos[k_x a/2-\pi(m-[q])\phi] \\ H_I(m)_{21}=2(\alpha_0+\alpha_3\beta)e^{ik_y b/2}\cos[k_x a/2-\pi(m-[q])\phi)] \\ H_I(m)_{22}=\alpha_1\beta+\alpha_2(\beta^2+2), \end{cases} \quad (8)$$

where $[q]=(q+1)/2$ is to set the origin at the center of each period q in each graphite layer. The diagonal matrix elements $H_I(m)_{11}$ and $H_I(m)_{22}$ are related to two atoms with the same (x,y) coordinate, so they are identical to those of without the magnetic flux. $\pi\phi$ in equation (8), which is the Peierls phase caused by the magnetic flux through one half of hexagon [26], is reflected in the nondiagonal matrix elements $H_I(m)_{12}$ and $H_I(m)_{21}$. Notably, the magnetic flux changes the phase from $k_x a/2$ to $[k_x a/2-\pi(m-[q])\phi]$. The H_J matrix comes from two atoms in the neighboring zigzag lines. The diagonal and nondiagonal matrix elements, $H_{J,11}$,$H_{J,22}$, and $H_{J,12}$, are vanishing. The only nonzero matrix element, which is the interaction between atom A_m and atom $B_{m\pm1}$, is

$$H_{J,21}=(\alpha_0+\alpha_3\beta)e^{-ik_y b}. \quad (9)$$

In the absence of the interlayer interactions, equations (7)–(9) describe the magneto-electronic properties of a monolayer graphite subjected to a perpendicular magnetic field [25,26].

The geometric structure of ABC-stacked graphite is shown in Figure 2. Half of the atoms are directly below the atoms in the adjacent layer and meanwhile directly above the hexagonal ring centers. This structure can be derived from the hexagonal structure by slipping every third layer. The periodical lengths along $\hat{x}$ and $\hat{y}$ are, respectively, $I_x = 2.42$ Å, and $I_y = \frac{3b}{2} = 2.13$ Å, the same as those in AA-stacked graphite. However, the periodical length along $\hat{z}$ is equal to $3c = 10.05$ Å. A primitive unit cell has six carbon atoms. The symmetric points are $\Gamma(0,0,0)$, $M(\frac{\pi}{a},\frac{\pi}{3b},0)$, $K(\frac{4\pi}{3a},0,0)$, $A(0,0,\frac{\pi}{3c})$, $L(\frac{\pi}{a},\frac{\pi}{3b},\frac{\pi}{3c})$, and $H(\frac{4\pi}{3a},0,\frac{\pi}{3c})$.

The tight-binding model is also used to evaluate the magneto-electronic structure of the ABC-stacked graphite. The site energy is zero, and the atomic hopping integrals β_i's are as follows (Fig. 2). β_0 represents the interaction between atom A and B on the same layer. β_4 is the interaction between the two atoms A (or two atoms B) from the two neighboring layers. When the atom A and B from the two neighboring layers have the same (x,y) coordinate, the interlayer interaction between them is β_1. If not, it is β_3. The parameters β_2 and β_5 describe the interaction between two atoms A, two atoms B, or atom A and B from the two next-neighboring layers. The interaction

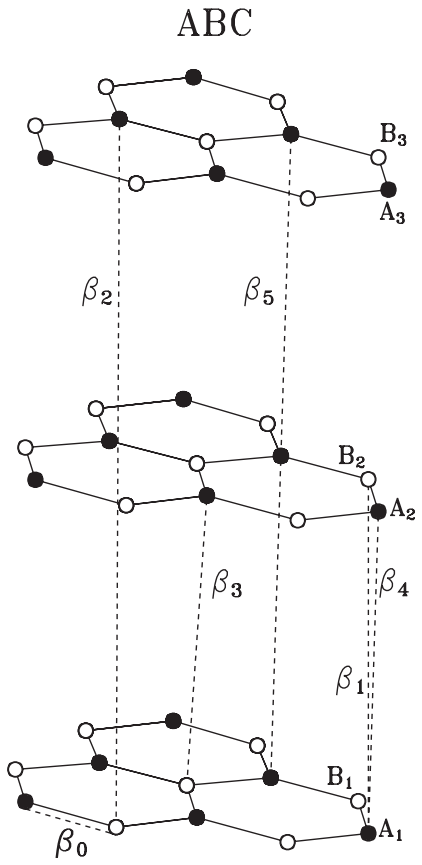

Fig. 2. Same plot as Figure 1, but shown for the ABC-stacked graphite.

is β_2 when atom A and B have the same (x, y) projection, and is β_5 otherwise. The values of interactions are: $\beta_0 = 3.16$ eV, $\beta_1 = 0.36$ eV, $\beta_2 = -0.02$ eV, $\beta_3 = 0.32$ eV, $\beta_4 = -0.03$ eV, and $\beta_5 = 0.013$ eV [9]. The Bloch function, the superposition of the six tight-binding functions, is

$$\Psi^h_{\mathbf{k}}(\mathbf{r}) = \mathrm{a}_1\Psi_{\mathbf{k},A_1} + \mathrm{b}_1\Psi_{\mathbf{k},B_1} + \mathrm{a}_2\Psi_{\mathbf{k},A_2} + \mathrm{b}_2\Psi_{\mathbf{k},B_2} + \mathrm{a}_3\Psi_{\mathbf{k},A_3} + \mathrm{b}_3\Psi_{\mathbf{k},B_3}. \quad (10)$$

In the basis of the Bloch function, the Hamiltonian matrix of the ABC-stacked graphite is

$$H_{ABC}(\phi = 0) = \begin{pmatrix} H_A & H_B & H_C \\ H_C & H_A & H_B \\ H_B & H_C & H_A \end{pmatrix}, \quad (11)$$

in which H_i denotes 2×2 matrix. The nonzero elements of H_A are

$$\begin{cases} H_{A,12} = \beta_0 f(k_x, k_y) \\ H_{A,21} = \beta_0 f^*(k_x, k_y), \end{cases} \quad (12)$$

and those of H_B $(=H_C^*)$ are

$$\begin{cases} H_{B,11} = (\beta_4 e^{ik_z c} + \beta_5 e^{-ik_z 2c}) f^*(k_x, k_y) \\ H_{B,12} = (\beta_1 e^{ik_z c} + \beta_2 e^{-ik_z 2c}) \\ H_{B,21} = (\beta_3 e^{ik_z c} + \beta_5 e^{-ik_z 2c}) f(k_x, k_y) \\ H_{B,22} = (\beta_4 e^{ik_z c} + \beta_5 e^{-ik_z 2c}) f^*(k_x, k_y). \end{cases} \quad (13)$$

The tight-binding function in the presence of the magnetic flux ($\phi = \phi_0/q$) is similar to that in equation (7). The Hamiltonian matrix, which is built from the extended $6q$'s tight-binding functions, is

$$\begin{pmatrix} H_I(1) & H_J(1) & 0 & \cdots & 0 & H_J^*(q) \\ H_J^*(1) & H_I(2) & H_J(2) & 0 & \cdots & 0 \\ 0 & \ddots & \ddots & \ddots & \ddots & \vdots \\ \vdots & \ddots & H_J^*(m) & H_I(m) & H_J(m) & \vdots \\ 0 & \ddots & \ddots & \ddots & \ddots & \ddots \\ H_J(q) & 0 & \cdots & 0 & H_J^*(q) & H_I(q) \end{pmatrix}, \quad (14)$$

in which H_I or H_J is a 6×6 matrix. The periodical boundary condition is $H_J^*(q+1) = H_J(1)$. H_I is spanned by the six tight-binding functions. It is associated with the interactions between two atoms in the mth zigzag line, from the same layer, the neighboring layers, or the next-neighboring layers. The nonzero elements of Hermitian H_I (H_J) are shown in the Appendix.

3 Magneto-electronic properties

The two-dimensional band structure of a monolayer graphite (Eq. (5)) is first reviewed. The occupied valence (π) bands are symmetric to the unoccupied conduction (π^*) bands about the Fermi level $E_F = 0$. The low energy dispersions near the K point are linear and isotropic. Furthermore, the valence and conduction bands just intersect at $E_F = 0$. Energy bands near the M and Γ points are parabolic and anisotropic dispersions. They, respectively, have energies $\pm\alpha_0$ and $\pm 3\alpha_0$ at the M and Γ points. The band width associated with the Γ point is $6\alpha_0$. The K, M, and Γ respectively belong to the local minimum point, the saddle point, and the maximum or minimum point in the energy-wave-vector space. Such special points would induce special structures in the density of states. The DOS due to the linear bands is vanishing at the Fermi level. The free carriers are absent, so that a monolayer graphite is a zero-gap semiconductor.

As shown in Figure 3a, the interlayer interactions play an important role in the electronic structure of the AA-stacked graphite. The occupied valence (π) bands are no longer symmetric to the unoccupied conduction (π^*) bands about the Fermi level, $E_F = 0.016$ eV. Energy dispersions are highly anisotropic; that is, there are stronger energy dispersions along $\hat{k_x}$ or $\hat{k_y}$ compared with those along $\hat{k_z}$. For a fixed k_z, energy dispersions in the k_x-k_y plane are similar to those of a monolayer graphite. That is to say, the local minimum point, the saddle point, and the maximum or minimum point are, respectively, at the zone corner (K), the middle point between two corners (H), and the center. The zone corner corresponds to the intersecting point of the linear bands; furthermore, conduction and valence bands in the k_x-k_y plane are symmetric to each other about this point. On the other hand, conduction and valence bands along $\hat{k}_z$ (or along the KH line)

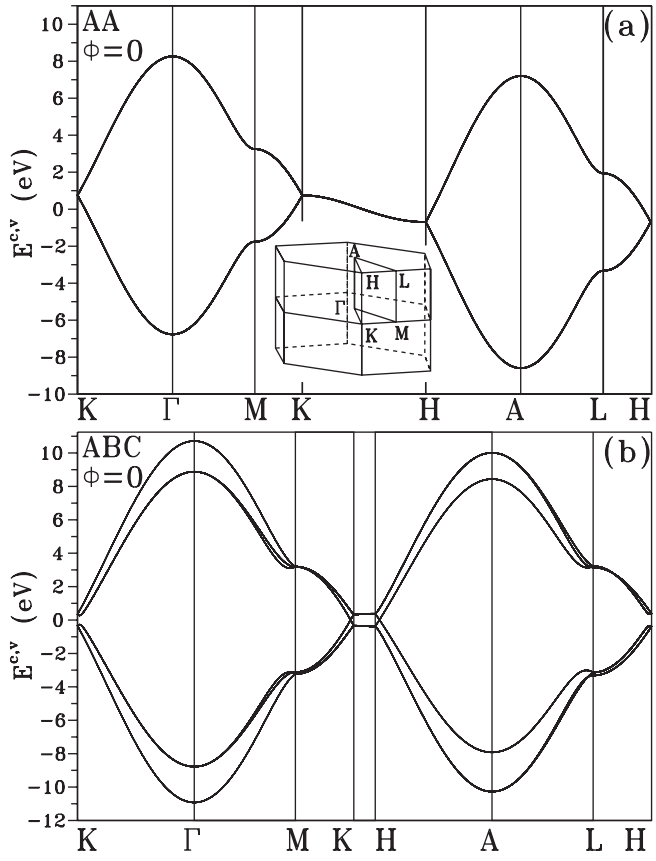

Fig. 3. Energy dispersions of the (a) AA- and (b) ABC-stacked graphites, and the hexagonal Brillouin zone in the inset.

would overlap each other near the zone corners. The Γ, M, K, A, L, and H points are the saddle points in the energy-wave-vector space except the maximum energy at the Γ point and the minimum energy at the A point. The band width, the energy difference between the maximum energy at the Γ point $(2(\alpha_1+\alpha_2)+3(\alpha_0+2\alpha_3))$ and the minimum energy at the A point $(-2(\alpha_1-\alpha_2)-3(\alpha_0-2\alpha_3))$, is $4\alpha_1+6\alpha_0$.

The low-energy electronic structure with band overlaps deserves a closer examination here. Such energy dispersions are near the zone corners. Along the KH line (Fig. 3a), the k_z-dependent energy dispersion is characterized by $2[\alpha_1\cos(k_zc)+\alpha_2\cos(2k_zc)]$. State energies of the K and H points are, respectively, $2(\alpha_1+\alpha_2)$ and $-2(\alpha_1-\alpha_2)$. As for the linear conduction and valence bands in the k_x-k_y plane at the intersecting K point, some valence-band state energies are higher than the Fermi level. It means that the interlayer interactions induce some free holes in the low-energy valence bands. The hole density decreases with the increase of k_z's. Free holes would change into free electrons when the state energy of the intersecting point is larger than the Fermi energy. The H point has the maximum electron density; that is, this intersecting point had the lowest energy compared with the those along the KH line. There are, respectively, hole and electron pockets near the K and H points. These two kinds of free carriers have the same density, and they are expected to play an important role in the essential physical properties, e.g., optical spectra, electronic excitations, and transport properties.

Energy dispersions of the ABC-stacked graphite are shown in Figure 3b. They exhibit the asymmetric structure about the Fermi level $E_F = 0.007$ eV and the high anisotropy. For the $KM\Gamma K$ plane of $k_z = 0$, the Γ, K, and M points are the maximum, local maximum or minimum, and saddle points, respectively. In general, energy dispersions are parabolic except those along the KM line ($k_z = 0$). There is a small energy spacing for the parabolic bands along the $K\Gamma$ line. The linear bands along the KM line would exhibit the weak overlap between valence and conduction bands. There are three conduction bands lower than the Fermi level, while the opposite is true of the three valence bands. Some free electrons and holes exist simultaneously near the K point. Similar energy dispersions could be found in the $HLAH$ plane of $k_z = \pi/3c$. However, the linear bands exist in the HA line, but not the HL line. The parabolic bands along the HL line exhibit a small energy spacing.

The stacking effect makes the ABC-stacked graphite quite different from the AA-stacked graphite in band structure. As for the former, it has the wider band width and exhibits the very weak k_z-dependence. There exist double and triple state degeneracies. The K and H points might exhibit the parabolic energy dispersions and have the small energy spacings. Valence and conduction bands overlap very weakly. Free electrons and holes survive at the K or H point simultaneously, but not at the K and H points, respectively.

The uniform perpendicular magnetic field, with the vector potential $\mathbf{A} = (-By, 0, 0)$, significantly modifies band structure of the AA-stacked graphite (Fig. 4). At $\phi = \phi_0/4$, the Hamiltonian is an 8×8 matrix, and the period along $\hat{k}_x$ is 1/4 of that without the magnetic flux. Energy bands are shown along $\Gamma X' MY\Gamma$ by the bold curves. Those at $\phi = 0$, obtained through the zone-folding method, are shown by the light curves for comparison. The k_z-dependence of energy dispersions is hardly affected by the magnetic flux. For example, energy bands along $X'M$ could be described by $2[\alpha_1\cos(k_zc)+\alpha_2\cos(2k_zc)]$+constant. The magnetic flux only leads to the rigid shift of the k_z-dependent energy bands. The chief cause is that the perpendicular magnetic field does not change the phases of the Hamiltonian matrix elements associated with k_z. On the other hand, the magnetic flux causes the special Landau levels and oscillating Landau levels for energy bands in the k_x-k_y plane, e.g., energy dispersions along $\Gamma X'$ and ΓY. It should be noted that the Landau levels might have partial flat or complete flat energy dispersions. The oscillating Landau levels and the partial flat Landau levels are, respectively, present at the low and high energies. Because of the Landau levels, the band width is drastically reduced by the magnetic flux, e.g., $E_D = 14.73$ eV $(=5.73\alpha_0)$ at $\phi = \phi_0/4$. The diminishing effect is enhanced with the increase of ϕ. Such an effect could also be found in the ABC-stacked graphite.

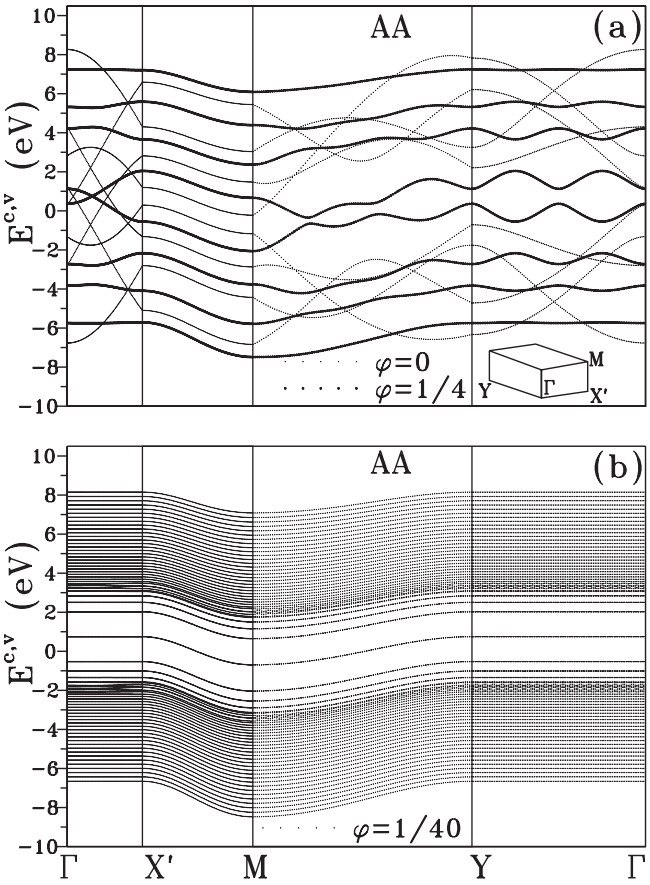

Fig. 4. Energy bands of the AA-stacked graphite along the symmetric points of the orthohombic Brillouin zone at (a) $\phi = 1/4\ \phi_0$ and (b) $\phi = 1/40\ \phi_0$.

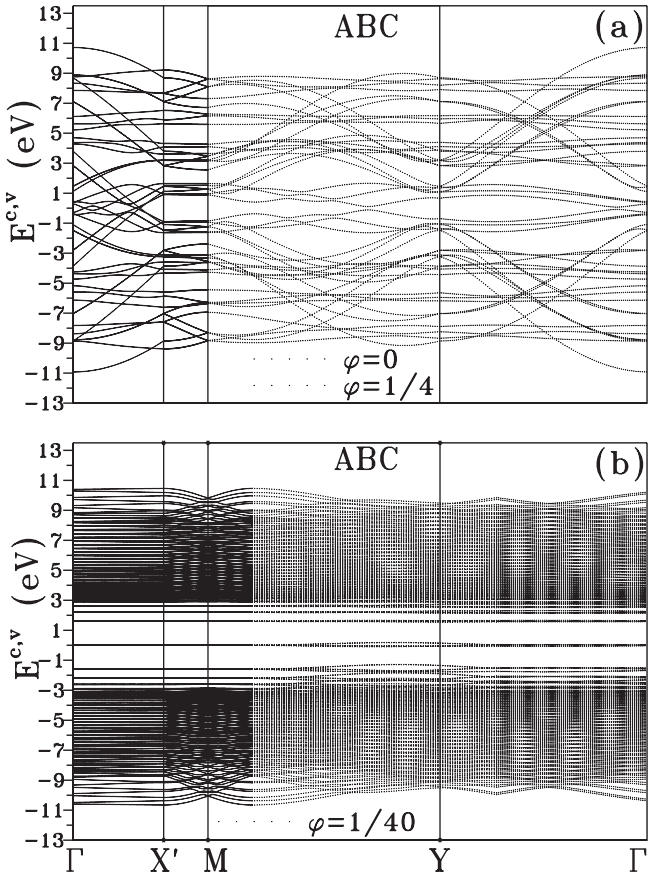

Fig. 5. Same plot as Figure 5, but shown for the ABC-stacked graphite.

When the magnetic flux is reduced, there are more complete flat Landau levels in the k_x-k_y plane, as shown in Figure 4b along $\Gamma X'$ and ΓY at $\phi = \phi_0/40$. Only some oscillating Landau levels survive at the low energy. There exists an energy spacings between two energy bands nearest to the Fermi level. However, the strong k_z-dependent energy dispersions make the AA-stacked graphite gapless or semimetallic. Notably, the AA-stacked graphite remains semimetallic in the presence of the magnetic flux. The number of symmetric points is largely enhanced as ϕ decreases. Such special points might be the saddle points, the local minima, and the local maxima. They would exhibit a lot of special structures in density of states.

The ABC-stacked graphite in the presence of ϕ also exhibits the Landau levels and the oscillating Landau levels in the k_x-k_y plane ($\Gamma X'$ and ΓY in Figs. 5a and 5b), as seen in the AA-stacked graphite. However, compared with those in the AA-stacked graphite (Figs. 4a and 4b), such levels have the stronger energy dispersions and the wider magnetoband width. Within the ABC-stacked graphite, half of carbon atoms in the two neighboring layers have different atomic positions. Therefore, the magnetic flux would induce the different phase differences between A atoms and B atoms in the neighboring layers. The mixing effect, due to the different phase differences, could explain why it is relatively difficult to observe the Landau behavior in the ABC-stacked graphite. The magnetic flux would further affect the k_z-dependence of energy dispersions, e.g., those along $X'M$.

The magnetoband structures would exhibit the butterfly-like energy spectra. The $1/\phi$- or q-dependent state energies are shown in Figures 6a and 6b for the Γ point. There are several discrete states at the high magnetic field, e.g., twenty discrete states at $\phi = \phi_0/10$. The energy spacings between two neighboring Landau levels are not identical to one another. This result means that the layered electron gas model can not describe the layered graphite. The discrete states would be getting into the continuous states as the magnetic field decreases. The latter are confined within 2.569 eV $\leq E^c \leq$ 7.7 eV or -6.4 eV $\leq E^v \leq -2.569$ eV (-9.1 eV $\leq E^v \leq -3.9$ eV) for the AA-stacked (ABC-stacked) graphite.

The density of states is very useful in understanding the essential physical properties, such as optical and electronic excitations. It is defined as

$$D(\omega;\phi) = \frac{2}{\pi} \sum_{h=c,v} \int_{1stBZ} \frac{d^3\mathbf{k}}{(2\pi)^3} \frac{\Gamma}{[E^h(\omega;\phi)^2 + \Gamma^2]}, \quad (15)$$

where $\Gamma = 0.026$ eV$(=0.01\alpha_0)$ is the broadening energy width. The special points in the energy-wave-vector space

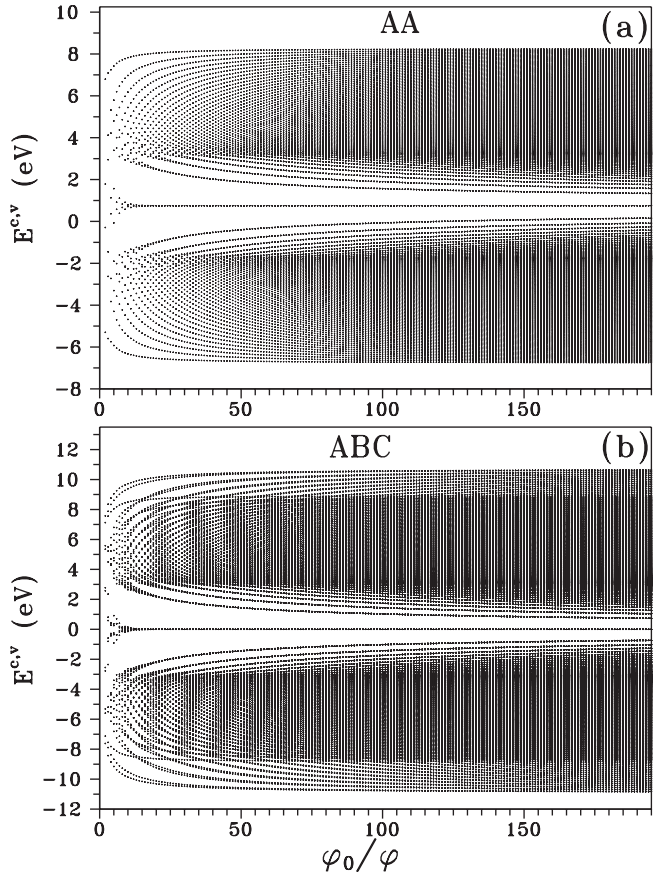

Fig. 6. The magnetic-flux-dependent energy spectra of the (a) AA- and (b) ABC-stacked graphites for the Γ point.

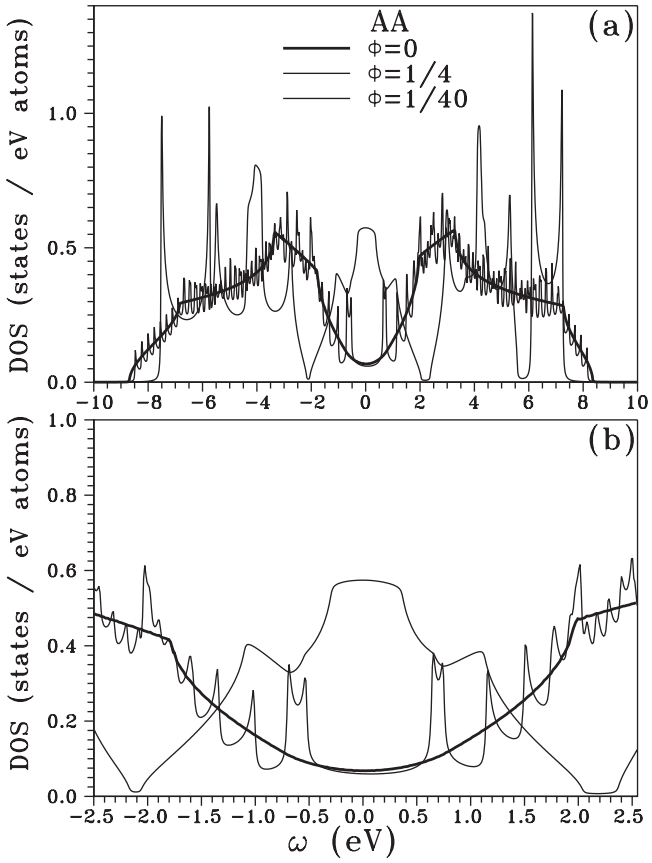

Fig. 7. (a) The density of states of the AA-stacked graphite at different ϕ's. Also shown in (b) are the low-frequency results.

would induce the special structures in DOS. Such structures directly reflect the main features of energy dispersions. They are dramatically altered by the external magnetic field. The special structures in DOS could be examined by the experimental spectroscopies, e.g., optical spectroscopies and STM.

At $\phi = 0$, DOS of the AA-stacked graphite, as shown in Figures 7a and 7b, exhibits eight special cusp structures, which are, respectively, located at -8.73 eV, -6.81 eV, -3.53 eV, -1.66 eV, 1.66 eV, 3.38 eV, 7.22 eV, and 8.31 eV. They correspond to the A, Γ, L, M, L, M, A, and Γ, respectively. The six points among them are the saddle points except the minimum energy at the A point and the maximum energy at the Γ point. All the cusp structures are associated with the saddle points, the minimum, and the maximum in the 3D energy-wave-vector space. The finite DOS at low energy suggests that the AA-stacked graphite is a semimetal.

At small ϕ, DOS exhibits a lot of special structures, e.g., DOS at $\phi = 1/40\ \phi_0$ in Figures 7a and 7b. Such structures are divergent in the square-root form. They come from the Landau levels in the k_x-k_y plane or the effective 1D parabolic bands along $\hat{k}_z$ (Fig. 4b). The 1D concave-upward (concave-downward) parabolic band would lead to the square-root divergences in the $1/\sqrt{\omega - E^h_{ed}}$ $(1/\sqrt{E^h_{ed} - \omega})$ form, where ω is the frequency and E^h_{ed} is the state energy at the h subband edge. The square-root peak structures would group together as ϕ grows. When the magnetic flux is high enough, there are $2q$'s groups of peak structures. At $\phi = 1/4\ \phi_0$, DOS displays four groups of peak structures at $\omega > 0$ or $\omega < 0$. The peak structures at large $|\omega|$'s just correspond to two pronounced square-root divergences, e.g., DOS at $\omega = -7.51$ eV and -5.74 eV; $\omega = 7.22$ eV and 6.13 eV. The double-peak divergent structures reflect the fact that the Landau levels, with large $|E^h|$'s, are almost flat (Fig. 4a) in the k_x-k_y plane, and they have the k_z-dependent energy dispersion due to the interlayer interactions. On the other hand, the low-frequency DOS exhibits the shoulder or cusp structures, which are related to the saddle points of the oscillating Landau levels. The oscillating Landau levels occur frequently at the low energy, so that DOS is largely enhanced.

DOS of the ABC-stacked graphite might differ from that of the AA-stacked graphite, as shown in Figures 8a–8b and 7a–7b. At $\phi = 0$, the former is almost equal to zero at $\omega \sim 0$, mainly owing to the weaker interlayer interactions. It exhibits the logarithmically divergent structures at $\omega = 3.20$ eV and -3.12 eV. The similar structures could be found in a 2D monolayer graphite at $\omega = \pm 3.16$ eV$(= \pm\ \beta_0)$. The main reason is that the state energies associated with the special points M and L are almost the same (Fig. 3b). At $\phi = 1/4\ \phi_0$, there are

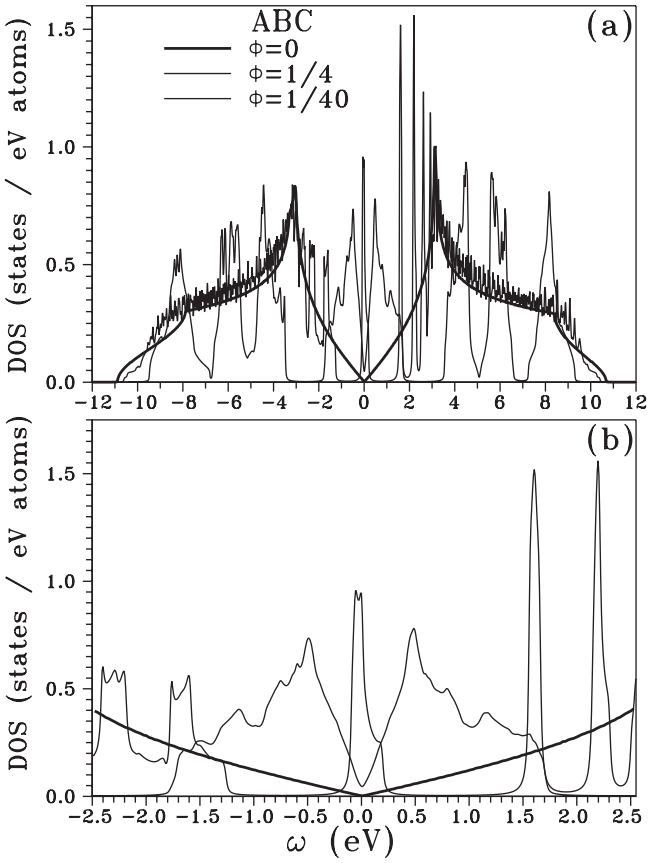

Fig. 8. Same plot as Figure 7, but shown for the ABC-stacked graphite.

eight groups of peak structure in DOS, and several wiggly peaks exist in each group. These two results further illustrate that the Landau levels have the weak wave-vector dependence in the k_x-k_y plane (Fig. 5a).

The comparison between a monolayer graphite [26] and the stacked graphites exhibits that the interlayer interactions have a great influence on the magneto-electronic properties. A monolayer graphite shows a symmetric magnetoband structure about the Fermi level, and so does the associated DOS. The main feature of magneto bands is sensitive to the magnitude of magnetic flux ϕ. At a small ϕ, energy dispersions of a monolayer graphite exhibits the 0D Landau levels in the $k_x - k_y$ plane and, therefore, DOS shows a lot of delta-function-like peaks. When the ϕ is high enough, e.g., $\phi = 1/4$, energy dispersions mainly exhibit 1D and 2D characteristics. The former are the 1D parabolic bands and the latter are the oscillating energy dispersions. The square-root peaks and logarithmic divergences, which are respectively associated with 1D and 2D energy dispersions, can be clearly found in DOS. The interlayer interactions significantly affects magnetoband structures of the layered graphites. They produce the k_z-dependent energy dispersions, destroy the band symmetry about the Fermi level, modify the energy dispersions in the $k_x - k_y$ plane, destroy the state degeneracy, change the energy spacing, widen the band width, and alter the symmetry points in the energy-wave-vector space.

The comparisons with the magneto-electronic properties of the AB-stacked graphite [27] is also made. At a strong magnetic field, magneto-band structures of the AB-stacked graphite exhibit 0D, 1D and 2D features (flat bands, 1D parabolic bands, and the oscillating bands). DOS shows the sharp peaks, square-root peaks, and logarithmic divergences, which are related to 0D, 1D and 2D energy bands. The lower the magnetic field is, the more Landau levels exist. DOS in the form of delta-function-like divergences (power-law divergences) below (above) E_F can be found at a small ϕ. The magnetic flux generates the Landau Levels and oscillating Landau subbands in the energy dispersions of the layered graphites. However, the stacking effects greatly influence the magneto-electronic properties. First, the layer graphites exhibit the quite different k_z-dependent energy dispersions, where the AA-stacked graphite show the cosine bands (Figs. 4a and 4b) while the AB- and ABC-stacked graphites exhibit the cosine and partial flat bands [27]. Moreover, the stacking effect affects the magnetoband structures in the $k_x - k_y$ plane, e.g., the main feature of energy bands, the oscillating period of the Landau subbands along $\hat{k}_x$ or $\hat{k}_y$, the subband spacings, the energy width, the DOS feature, and the special structures in DOS.

4 Conclusions

Magneto-electronic properties of the AA- and ABC-stacked graphites are investigated within the frame of tight-binding method. The comparisons with a monolayer graphite and the AB-stacked graphite are also made. Magneto-electronic properties are mainly determined by the interlayer interactions, the magnetic field, and the stacking sequences. The main features of energy bands are directly reflected in density of states. The predicted results could be verified by the STM and the optical spectroscopy.

Firstly, the interlayer interactions would change the energy dispersions, destroy the band symmetry about the Fermi level, induce the overlap between valence and conduction bands, widen the band width, and alter the symmetry points in the energy-wave-vector space. Secondly, the magnetic field introduces the Peierls phase in the Bloch functions and thus strongly modifies the energy dispersions of the Landau Levels, the subband spacings, the energy width, and the special structures in DOS. When the magnetic flux is reduced, there are more Landau levels, and the band width is widened. In the presence of the magnetic flux ϕ, DOS could exhibit the cusps, the logarithmical divergent peaks, and the square-root divergent peaks, which, respectively, come from the effective 3D, 2D, and 1D energy dispersions. The effective 1D Landau levels could induce several groups of peak structure for the sufficiently high magnetic flux. Thirdly, the stacking sequences dominate over the low-energy band overlap and the anisotropy of energy bands. There are certain important differences between the AA-, AB- and ABC-stacked

$$\begin{cases} H_{I,12} = H^*_{I,21} = 2\beta_0 e^{-ik_y b/2}\cos[k_x a/2 - \pi(m-[q])\phi] \\ H_{I,13} = H^*_{I,31} = 2Z_1 e^{ik_y b/2}\cos[k_x a/2 - \pi(m-[q]-1/3)\phi] \\ H_{I,14} = H^*_{I,41} = Z_3 \\ H_{I,15} = H^*_{I,51} = 2Z^*_1 e^{-ik_y b/2}\cos[k_x a/2 - \pi(m-[q])\phi] \\ H_{I,16} = H^*_{I,61} = Z^*_2 e^{-ik_y b} \\ H_{I,23} = H^*_{I,32} = Z_2 e^{ik_y b} \\ H_{I,24} = H^*_{I,42} = 2Z_1 e^{ik_y b/2}\cos[k_x a/2 - \pi(m-[q])\phi] \\ H_{I,25} = H^*_{I,52} = Z^*_3 \\ H_{I,26} = H^*_{I,62} = 2Z^*_1 e^{-ik_y b/2}\cos[k_x a/2 - \pi(m-[q]+1/3)\phi] \\ H_{I,34} = H^*_{I,43} = 2\beta_0 e^{-ik_y b/2}\cos[k_x a/2 - \pi(m-[q]-1/3)\phi)] \\ H_{I,35} = H^*_{I,53} = Z_1 e^{-ik_y b} \\ H_{I,45} = H^*_{I,54} = 2Z_2 e^{-ik_y b/2}\cos[k_x a/2 - \pi(m-[q]\phi)] \\ H_{I,46} = H^*_{I,64} = Z_1 e^{-ik_y b} \\ H_{I,56} = H^*_{I,65} = 2\beta_0 e^{-ik_y b/2}\cos[k_x a/2 - \pi(m-[q]+1/3)\phi], \end{cases} \quad (16)$$

graphites such as the low energy dispersion, the state degeneracy, the energy width, the free carriers, the Landau levels or the oscillating Landau levels, and the special structures in DOS. Above all, the Landau levels in the layered graphites might quite differ from those of a 2D electron gas.

The authors gratefully acknowledge the support of the Taiwan National Science Council under the contract No. NSC 95-2112-M-165-001.

Appendix

The nonzero elements of Hermitian H_I and H_J are shown as follows

see equation (16) above

where $Z_1 = (\beta_4 e^{ik_z c} + \beta_5 e^{-ik_z 2c})$, $Z_2 = (\beta_3 e^{ik_z c} + \beta_5 e^{-ik_z 2c})$, and $Z_3 = (\beta_1 e^{ik_z c} + \beta_2 e^{-ik_z 2c})$. Z_i's are related to the interlayer interactions. $\pm\frac{\pi\phi}{3}$ in equation (A.1) is due to the coordinate difference in two centers of the neighboring planes. The nonzero elements of the off-diagonal matrix H_J are

$$\begin{cases} H_{J,13} = Z_1 e^{-ik_y b} \\ H_{J,23} = 2Z_2 e^{-ik_y b/2}\cos[k_x a/2 - \pi(m-[q]+1/3)\phi] \\ H_{J,24} = Z_1 e^{-ik_y b} \\ H_{J,51} = Z^*_1 e^{-ik_y b} \\ H_{J,53} = 2Z^*_1 e^{-ik_y b/2}\cos[k_x a/2 - \pi(m-1-[q]+1/3)\phi] \\ H_{J,54} = Z^*_2 e^{-ik_y b} \\ H_{J,61} = 2Z^*_2 e^{-ik_y b/2}\cos[k_x a/2 - \pi(m-[q]-1/3)\phi] \\ H_{J,62} = Z_1 e^{-ik_y b} \\ H_{J,63} = Z^*_3 \\ H_{J,64} = 2Z_1 e^{-ik_y b}\cos[k_x a/2 - \pi(m-[q]-1/3)\phi]. \end{cases} \quad (17)$$

References

1. P.R. Wallace, Phys. Rev. **71**, 622 (1947)
2. R. Haering, Can. J. Phys. **36**, 352 (1958)
3. J.C. Slonczewski, P.R. Weiss, Phys. Rev. **109**, 272 (1958)
4. J.W. McClure, Carbon **7**, 425 (1969)
5. K. Nakao, J. Phys. Soc. Jpn **40**, 761 (1976)
6. J.C. Charlier, J.P. Michenaud, X. Gonze, J.P. Vigneron, Phys. Rev. B **44**, 13237 (1991)
7. J.C. Charlier, X. Gonze, J.P. Michenaud, Phys. Rev. B **43**, 4579 (1991)
8. J.C. Charlier, J.P. Michenaud, X. Gonze, Phys. Rev. B **46**, 4531 (1992)
9. J.C. Charlier, J.P. Michenaud, P. Lambin, Phys. Rev. B **46**, 4540 (1992)
10. J.C. Charlier, X. Gonze, J.P. Michenaud, Carbon **32**, 289 (1994)
11. M. Aoki, H. Amawasi, Solid State Commun. **142**, 123 (2007)
12. G. Dresselhaus, Phys. Rev. B **10**, 3602 1974
13. W.W. Toy, M.S. Dresselhaus, G. Dresselhaus, Phys. Rev. B **15**, 4077 (1977)
14. T. Matsui, H. Kambara, Y. Niimi, K. Tagami, M. Tsukada, H. Fukuyama, Phys. Rev. Lett. **94**, 226403 (2005)
15. S. Chehab, K. Guerin, J. Amiell, S. Flandrois, Eur. Phys. J. B **13**, 235 (2000)
16. W.T. Pong and C. Durkan, J. Phys. D: Appl. Phys. **38**, R329 (2005)
17. K.S. Novoselov, A.K. Geim, S.V. Morozov, D. Jiang, Y. Zhang, S.V. Dubonos, I.V. Grigorieva, A.A. Firsov, Science **306**, 666 (2004)
18. J.S. Bunch, Y. Yaish, M. Brink, K. Bolotin, P.L. McEuen, Nano. Lett. **5**, 287 (2005)
19. C. Berger, Z. Song, T. Li, X. Li, A.Y. Ogbazghi, R. Feng, Z. Dai, A.N. Marchenkov, E.H. Conrad, P.N. First, W.A. de Heer, J. Phys. Chem. B **108**, 19912 (2004)
20. K.S. Novoselov, A.K. Geim, S.V. Morozov, D. Jiang, M.I. Katsnelson, I.V. Grigorieva, S.V. Dubonos, A.A. Firsov, Nature **438**, 197 (2005)
21. Y. Zhang, Y.W. Tan, H.L. Stormer, P. Kim, Nature **438**, 201 (2005)
22. C.L. Kane, E.J. Mele, Phys. Rev. Lett. **95**, 226801 (2005)
23. F. Guinea, A.H. Castro Neto, N.M.R. Peres, Phys. Rev. B **73**, 245426 (2006)
24. R. Rammal, J. Phys. **46**, 1345 (1985)
25. K. Wakabayashi, M. Fujita, H. Ajiki, M. Sigrist, Phys. Rev. B **59**, 8271 (1999)
26. C.P. Chang, C.L. LU, F.L. Shyu, R.B. Chen, Y.K. Fang, M.F. Lin, Carbon **42**, 2975 (2004)
27. C.P. Chang, C.L. LU, F.L. Shyu, R.B. Chen, Y.C. Huang, M.F. Lin, Carbon **43**, 1424 (2005)